Hochschule
Bonn-Rhein-Sieg

DLR

Department: Ingenieurwissenschaften und Kommunikation (IWK)
Study program: „Nachhaltige Ingenieurwissenschaft“ (B.Eng.)

Bachelor-Thesis (abridged version)

“ Life Cycle Assessment of Particle Based and Monolithic Redox Reactors using Concentrated Solar Power for Hydrogen Production “

Presented by:
Simon Philipp Adams
[redacted]

First examiner: Prof. Dr. Stefanie Meilinger
Second examiner: Prof. Dr. Anna-Lena Menn

Wachtberg, 19.02.2025

Abstract

As global warming and human intervention into ecological systems continue, the need of sustainable hydrogen production pathways is growing as well. This study addresses a framework for evaluating the environmental impact of two innovative production technologies based on thermochemical redox cycles. This is done by performing a life cycle assessment (LCA) based on international standardizations. As both analyzed concepts have not been realized in a large scale yet, a methodology is developed for approximating the component dimensions and material flows to gather inventory data. This methodology is implemented in Brightway2 / Activity Browser and parametrized for flexibility. Most important components are worked out in terms of their environmental impact as well as the sensitivity of certain parameters on the results. Given that, advices for the focus of further research can be provided to assess the technologies in more detail.

Hochschule Bonn-Rhein-Sieg

DLR

Table of Contents

List of Figures

List of Abbreviations

abbreviation	meaning
CSP	Concentrated Solar Power
DNI	Direct Normal Irradiance
EoL	End of Life
GLO	Global
GWP	Global Warming Potential
ISO	International Organization for Standardization
LCA	Life Cycle Assessment
LCIA	Life Cycle Impact Assessment
LOP	Agricultural Land Occupation Potential
RoW	Rest of the World
WCP	Water Consumption Potential

Abbreviations used for component layout:

abbreviation	meaning
ASG	aperture steam generation
cm	ceramic membrane
HX	heat exchanger
ins	insulation
ITM	ion transport membrane
lt	lifetime
OW HX	oxygen-water heat exchanger
ox	oxidation reactor
rec	receiver
red	reduction reactor
res	residence (time)
RM	redox material
RMA	redox material assembly
stf	solar-to-fuel
SHR	steam heat recovery
ts	transport system(s)
VP	vacuum pump

1 Introduction

> *“ Humanity has the ability to make development sustainable - to ensure that it meets the needs of the present without compromising the ability of future generations to meet their own needs.” (Brundtland et al., 1987, p. 24)*

Since decades, the reduction of greenhouse gas emissions and ecological impact caused by human interventions have been discussed at international conferences (Cho et al., 2023). Yet, annual global surface temperature anomalies are still rising (National Oceanic and Atmospheric Administration, 2025) and nearly 8 gigatons of CO_2 were globally emitted in the mobility sector alone in 2022 (François et al., 2024). To counteract global warming, the European Union has set the goal to reduce carbon emissions by 40% until 2030 compared to the year 1990 (Chelvam et al., 2024). Widening the view on other aspects of sustainability, the 2030 Agenda for Sustainable Development was unanimously adopted by the United Nations in 2015, presenting the Sustainable Development Goals (SDG) (United Nations, 2025). Besides other important goals, clean energy, innovation in industry and infrastructure as well as climate action and sustainable cities and communities are topically addressed by the SDGs. Apart from clean energy production, the work towards these goals stagnated or regressed according to the last report of the United Nations by a considerable amount (United Nations General Assembly, 2024).

Renewable hydrogen is increasingly studied, as it can resemble a low-carbon energy carrier not only for heat supply, but for replacing fossil transport fuels as well (Cho et al., 2023). This rising trend in interest can also be seen in the temporal distribution of national hydrogen strategy announcements, from which 40% refer to the SDG framework (Strelkovskii and Komendantova, 2025). As most hydrogen is currently produced by fossil technologies like steam methane reforming (SMR) or coal gasification (CG), a shift towards green production pathways is needed in order to meet sustainability as defined by (Brundtland et al., 1987). Furthermore, there seems to be a mismatch between the prognosed hydrogen production rate and demand in 2030 (Cho et al., 2023; Kodgire, 2025), underlining the need of further research about H_2-production processes.

The focus of this thesis are two innovative production processes based on the concept of thermochemical redox cycling. The heat utilized in these processes is coming from concentrated solar radiation, thus, presenting a renewable source for green hydrogen or syngas production (Weber et al., 2023). Furthermore, the two concepts (distinct in redox material shape) are promising high theoretical efficiencies (Brendelberger et al., 2022), motivating further research on the topic. The study is written at the Institute of Future Fuels, which is part of the German Aerospace Center (DLR) and target group of the LCA. The research focus of the institute lies on the development and evaluation of CO_2-neutral production pathways of synthetic fuels (Institute of Future Fuels, 2025a). The thesis is assigned to the SOLHYKO project, which is part of the department for the evaluation of solar production processes. In this project, the production of H_2 or syngas through thermochemical redox cycling and solar reforming is developed and evaluated (Institute of Future Fuels, 2025b). Thereby, this study addresses the evaluation of environmental impact of the redox-cycle-based systems. This evaluation is done by performing a life cycle assessment (LCA) of both systems. The LCA is based on the ISO norms 14040 and 14044, as they resemble a standardized concept which most industry-related LCA studies are compliant with (Rihner et al., 2025). The results of an LCA can be used to identify the most important contributors to the environmental impact of a system in a quantitative way. This allows for a better decision making in the design phase of a product development process (Chang et al., 2014). As the development of the analyzed systems is in a relatively early stage however and not many studies have been conducted about its environmental impact (Kafle et al., 2025), the statements drawn in this thesis will not account for recommendations for action. Instead, a workflow for the conduction of an LCA about the two systems is presented. The main research questions are the following:

1. How can a flexible LCA-workflow look like for approximating the environmental impact of both analyzed systems iteratively?
2. How can the inventory data of both technologies be predicted?
3. What are the most impactful components in terms of environmental impact and which parameters are the most sensitive to the LCIA?

2 Background

The two analyzed systems are based on thermochemical redox cycling.
For a better understanding, the chemical and physical principles as well as basic components of the analyzed systems are shown here. Furthermore, the most important differences between both systems are pointed out. The thermochemical cycles are based on two reactions, namely the reduction and oxidation of a redox material. This material can either be volatile or non-volatile. The redox material included in this study is cerium oxide, which is non-volatile and non-stoichiometric. (Chen et al., 2023) The chemical reactions for this case are shown in equations (1) and (2) (Le Gal et al., 2022):

$$M_xO_y \rightarrow M_xO_{y-\delta} + \frac{\delta}{2}O_2 \quad (1)$$

$$M_xO_{y-\delta} + \delta H_2O \rightarrow M_xO_y + \delta H_2 \quad (2)$$

When splitting CO_2 instead of water, carbon monoxide can be produced as well to gain syngas (Weber et al., 2023a). The reduction extent δ is depending on the reduction temperature and partial oxygen pressure and should be as high as possible (Bulfin et al., 2013; Chen et al., 2023). The redox material can be stationary or moving. For the latter, the redox material is either in the shape of particles or monolithic structures. (Chen et al., 2023). An important characteristic of solar thermochemical hydrogen production systems is the solar-to-fuel efficiency. It can be defined using equation (3) (Weber et al., 2023):

$$\eta_{stf} = \frac{HHV_{H_2} \times \dot{n}_{H_2}}{\dot{Q}_{rec}} \quad (3)$$

Concentrating the solar radiation can either be achieved by parabolic trough collectors, heliostat fields, linear Fresnel reflectors or parabolic dishes (Chen et al., 2023). In the case of this study, heliostat fields in combination with a tower are proposed for concentrating the sunrays onto the receivers.

Both systems include a reduction and oxidation reactor as well as a transport mechanism for the metal oxide. Furthermore, the reactors are insulated to a certain degree to prevent thermal deficiencies. (Brendelberger, 2024; Weber et al., 2023).

For better comparability, heat recovery throughout the redox material cycle is implemented for both systems in this study.

A visual overview of the analyzed systems is shown in Figure 1.

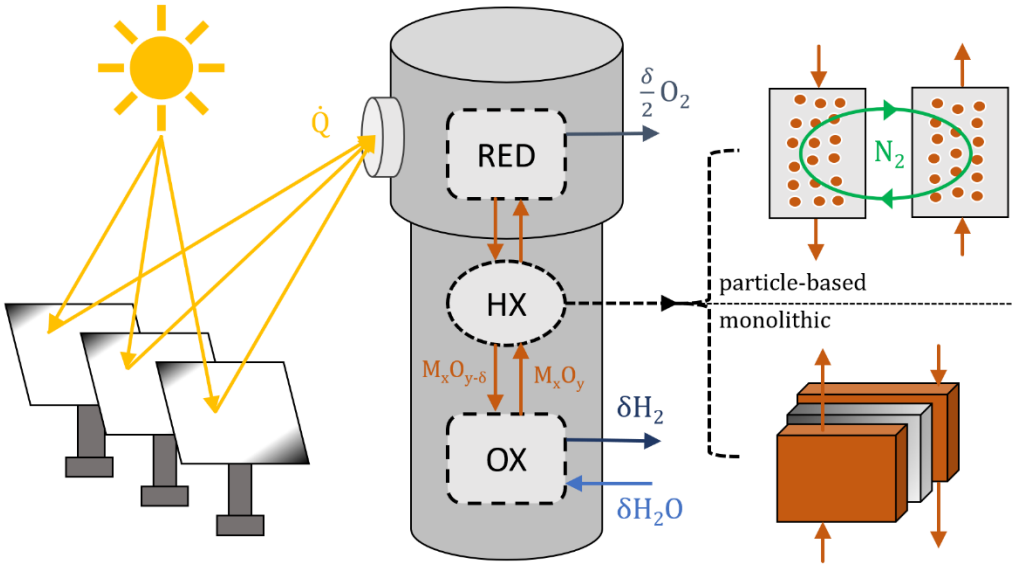

Figure 1: Overview of monolithic and particle-based system (Brendelberger et al., 2022; Weber et al., 2023)

2.1 Monolithic System

In the monolithic system, a redox material assembly (RMA) consisting of multiple monolithic structures is being used. These monoliths are transported linearly and back and forth between the reduction- and oxidation reactors. In between, gates are placed to prevent unwanted oxygen leakage into the reduction reactor. The reduction reactor is proposed to have multiple apertures. (Brendelberger et al., 2022)

Important process parameters are the reaction temperatures, oxygen partial pressure at the reduction step, cycle duration and the dimensions of the RMA for example. Radius and height as well as the number of redox material assemblies can affect the efficiency as these parameters influence the heat transfer into the metal oxide. (Brendelberger, 2024)

2.2 Particle-Based System

As the name of this concept suggests, the redox material is formed into small particles with a diameter of around 2 mm instead of having monolithic structures (Weber et al., 2023). These particles are falling naturally through the reduction reactor, heat exchanger and oxidation chamber. In place of having apertures at the reduction reactor, receivers are used which rotate to heat the particles evenly. Transporting the particles back to the top can be done by using a bucket elevator or a rotating elevator casing (Chen et al., 2023). For this system, important parameters are the reaction temperatures & partial oxygen pressure as well. Furthermore, the bed radius, bed porosity, filling percentage, particle velocity and residence time are of interest. (Weber et al., 2023)

To adapt for the desired power, either the dimensions of the receiver can be changed, or multiple receivers are used (as shown in this study).

2.3 Key Differences between both Systems

Besides the differences in redox material shaping as well as the transport mechanisms used to cycle the metal oxide, another relevant difference is the principle by which the oxygen released in the reduction chamber is extracted.

In the monolithic system, a vacuum pump is being used to create a negative pressure. Thereby, the oxygen which is split of the redox material is pumped out. (Brendelberger, 2024). There are different options for vacuum pumping, including mechanical-, jet- and thermochemical pumps (Brendelberger et al., 2017). The oxygen must be cooled down however before entering the pumping system. The exchanged heat could be used in another process inside of the system.

In the particle-based system on the other hand, a sweep gas is blown across the reduced particles to directly carry away the oxygen in a separate cycle. Afterwards, the sweep gas (e.g. nitrogen) is cleaned by an ion transport membrane to filter out the oxygen.

A compressor is used to accommodate for the pressure drop throughout the components. If the sweep gas leaks away through the receiver for example, an air separation unit might be needed to regain sweep gas. (Weber et al., 2023)

3 Methodology

This chapter includes the procedure and methods that are used for conducting the study. It contains the method for deriving the dimension of system components as well as the standardized LCA-Framework that the study is based on. Furthermore, the software used for inventory calculation and impact assessment is presented.

3.1 LCA-Framework

To ensure transparency and comparability to other LCA studies, the norms 14040 and 14044 of the International Organization for Standardization are taken as guidelines to perform the life cycle assessment. These norms provide a framework which is shown in this sub-chapter. An LCA can be split up into four main sections, which are outlined in Figure 2. Although chapter-names in this thesis are not strictly following ISO-standards, the content should be complying. To remain traceability, the connection between the chapters and the structure according to the norms is shown in this sub-chapter as well.

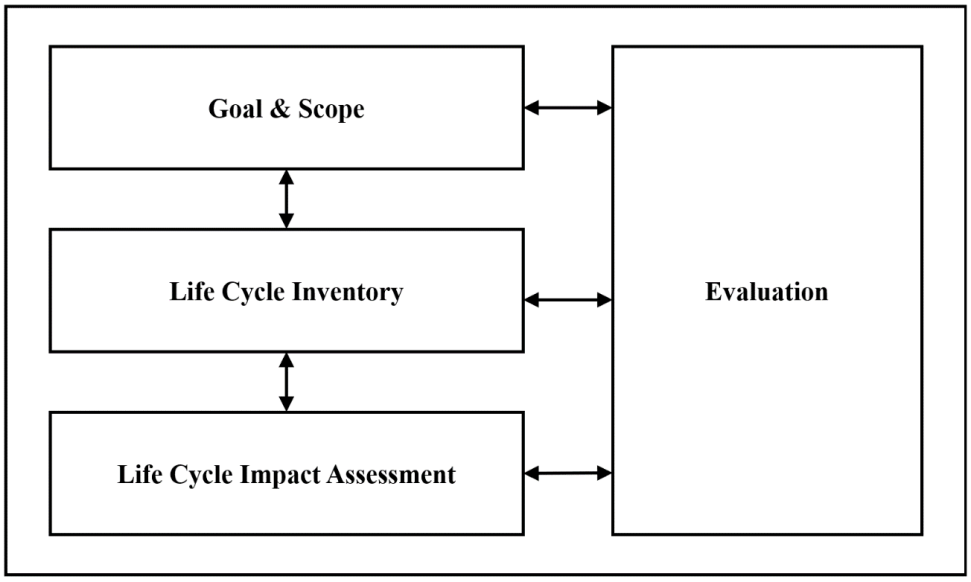

Figure 2: LCA-Framework
(DIN EN ISO 14040, 2021)

First, goal and scope of the assessment need to be defined. The scope is defined by presenting system boundaries and process flow charts, which point out what material or energy flows and emissions to the environment are considered. The life cycle stages, which are covered by the assessment, should be clarified. Motivation and target group of the assessment should be named. In addition to that, a functional unit is defined, describing on what the LCA-results should be normalized. This could, for example, be a lifetime or production rate of a product. Furthermore, primary and secondary data sources as well as assumptions made throughout the assessment process should be pointed out.
While motivation and target group of the assessment are shown in chapter one, the scope of the analysis is presented in chapters three and four. Chapter two contains information about the physical functionality of the systems, while chapter four characterizes the system boundaries. In chapter 3.3 the choice of impact assessment is shown while in chapter five, data sources and assumptions of the LCA are described.
In the life cycle inventory, relevant in- and output flows of the system are shown and described. This includes emissions as well as materials and can be seen in chapter 6.1.
The life cycle impact assessment contains the presentation of results which have been conducted by applying an LCIA method onto the modelled system. These results can either be divided into mid- or endpoint impact categories. Hereby, midpoint refers to defined emission-equivalents which have a certain environmental impact, while endpoint categories are specific combinations of emissions contributing to one effect, e.g. human health. This step is fulfilled by chapter 6.2, in which the components are ranked.
Last but not least, the results are evaluated and interpreted. Thereby, most contributing processes can be revealed, and the overall impact can be compared to similar products or technologies. This is covered in chapter 6.2 and 7. Furthermore, data quality and the sensitivity of certain parameters on the LCIA are evaluated, as shown in chapters 7 and 6.3. The LCA-process is to be seen as iterative, meaning over the course of conducting the study, goal and scope are adjusted, leading to new LCA-results.
(DIN EN ISO 14040, 2021; DIN EN ISO 14044, 2021)

3.2 LCA-Software

To perform the LCA the software package Brightway2 was used. It is written in Python® and was designed to easily handle large datasets fast and accurately, while allowing flexibility (Brightway Developers, 2025). The biosphere-database is created by it for new projects, including elementary flows (Mutel, 2017). To acquire the information needed for inventory implementation in Brightway2, the ecoinvent database was used, which has been developed since more than two decades now (Frischknecht and Rebitzer, 2005).
The imported version used is 3.9.1, released in 2022 (ecoinvent, 2025). To work with the software package, the Activity Browser was used. This program has two main purposes, namely providing a graphical user interface to Brightway and allowing extension to modelling approaches through graphical representation. It can not only be used to manage Brightway projects and calculate LCA results, but also to analyze uncertainty and sensitivity or parametrizing different flows. Furthermore, Sankey Diagrams and Monte Carlo analysis can be run. (Steubing et al., 2020; Steubing and Visscher, 2025)
Figure 3 shows different sections and tabs in the Activity Browser, e.g. database overview or LCA setup, to easily work on different projects (Steubing et al., 2025).

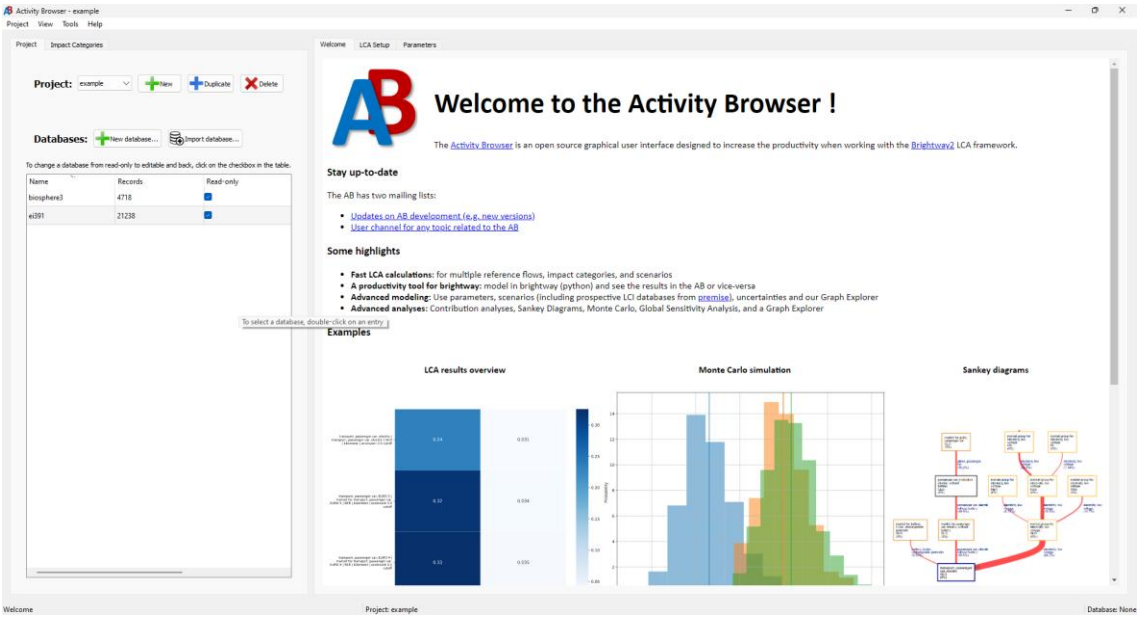

Figure 3: Start-up screen of an exemplary project in Activity Browser

3.3 Impact Assessment Method

The methods chosen to perform the impact assessment are ReCiPe 2016 v1.03 midpoint (H) no LT as well as EF v3.1. This way mainly the choice because of further research at DLR using similar methods and the fact that many different environmental impacts can be covered. For the Global Warming Potential, Environmental Footprint was used.
The results are normalized to the functional unit. As not all midpoint categories can be analyzed in detail due to time constraints, a selection was made. Three impact categories are mainly described: Global Warming Potential, Agricultural Land Occupation Potential and Water Consumption Potential. The GWP is of interest, as most LCA-studies include it (Chelvam et al., 2024) and it therefore serves as a good way to validate the outcomes of the LCA. The LOP was chosen, as biomass-related H_2-production methods can be competing in land occupation with food crops (Emetere et al., 2024). Furthermore, concrete is contained a lot throughout concentrated solar power plants. As concrete can have over 70% of its related foreground processes (processes which the decisionmaker of a product has influence on) contributing to the impact on land occupation (Feng et al., 2023), it is interesting to see how other materials and components used in the redox reactor systems would perform in that regard. The WCP was analyzed, as potential locations for concentrated solar power plants are expected to be areas with scarce water compared to other locations in the world. As other impact categories can also have a lot of building material foreground-processes related to them (Feng et al., 2023), they are evaluated as well, but not as detailed. For a better overview of all impact categories, the average impact contributions of the components of both systems are determined. These values are obtained by taking the relative contribution of one component to the complete impact in one category and then averaging these relative contributions along all impact categories for each component. This approach is explained in the attachments for better understanding. In all LCIA-related diagrams, every component is shown by its production phase and End-of-Life, with the latter being indicated by “EoL” written behind it. If the component is contributing to the use phase, it is indicated by the word “operation”.

3.4 Geometric Component Layout

To acquire the required information for the LCA, the amount of each material used inside the systems must be determined. This is done by researching the model layout of each component, e.g. by literature or talking to colleagues at DLR.

These models are then transformed into simple geometric shapes, like a cylinder or cube for example. This not only allows reduction in complexity but also makes it possible to derive equations that describe the volume and area of the components. Thereby, the equations can be put into Brightway. By doing so, parametrization is made easier to adapt to future research progress in the possible scale-up of the discussed technologies.

For instance, if a more detailed model was to be found by researchers and the radius of the components is known, it can be changed in the LCA-Software and a new LCA could be run to evaluate the environmental impact.

An example of such a geometrical simplification is shown in Fig. 4.

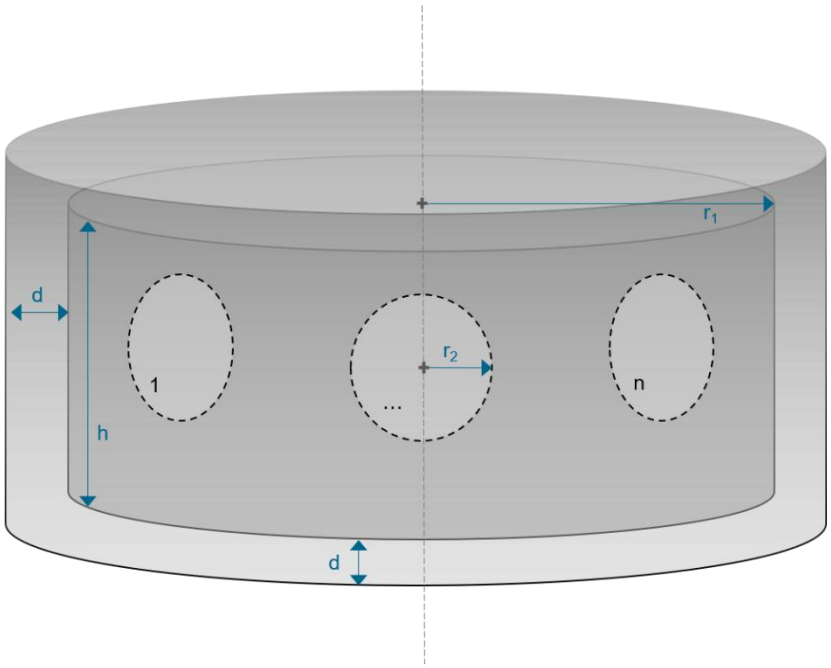

Figure 4: Exemplary geometrical simplification of a component

In this example, shapes are assumed to be cylindrical. A cavity with radius r_1 and insulation thickness d has a height of h and n number of cutouts, each with a radius r_2. The area of a circle and the volume of a cylinder are described by equations (1) and (2):

$$A_{circle} = \pi \times r^2 \quad (1)$$

$$V_{cylinder} = \pi \times r^2 \times h \quad (2)$$

Adapting those formulas to the example leads to equations (3) and (4):

$$A_{casing} = \pi \times r_1 \times 2 \times \left(r_1 + (h + 2d)\right) - n \times \pi \times r_2^2 \quad (3)$$

$$V_{insulation} = \pi \times ((r_1 + d)^2 \times (h + 2d) - r_1^2 \times h - n \times r_2^2 \times d) \quad (4)$$

For each component that could be described in such a simplified way, formulas were put into the corresponding parameter declarations. For the monolithic system, this was carried out for the reduction and oxidation reactors, the gates, transportation systems and the redox material heat exchanger. The geometrically simplified components inside of the particle-based system are the reduction and oxidation reactor, the transport system, pre-heating heat exchanger, ion transport membrane as well as the receivers.
Detailed information about the geometric assumptions and formulas used for calculating volumes and surface areas are provided in the attachments.

3.5 Dimensioning of Solar Field and Tower

As the main focus of this study is to evaluate the environmental impact of the new redox reactor concepts and create LCA-models of them in Brightway, the heliostat fields and solar tower of both systems are not modelled anew. Instead, a dataset of the ecoinvent database which is based on the dissertation of (Telsnig, 2015) is used.

However, as the inventory presented in the dissertation and used in the dataset is designed for electricity generation through concentrated solar power, it is adapted by leaving out the molten salt storage or power block for example. To account for the difference in efficiency and heat required at the receiver, the solar field and tower size are scaled accordingly. To achieve that, multiple studies containing data about CSP-plants have been evaluated to derive an average mathematical relationship between the electrical power of those plants and the solar field area. As the dataset is valid for 20 MW of electrical power, the processes connected to it are scaled regarding the calculated theoretical power needed in the analyzed systems. The solar field area is determined by the DNI, the daily operational hours and the optical efficiency, as shown in equation (5):

$$A_{solarfield} = \frac{\dot{Q}_{rec} \times t_{op} \times 365 \frac{d}{a}}{\eta_{opt} \times DNI} \quad (5)$$

To determine the tower height of both analyzed systems, the relationship between solar field area and tower height given in literature was evaluated. Thereby, the tower height is only used for considering the piping inside of them.

4 System Boundaries

In this chapter, the system boundaries of the analyzed systems are presented.
First, a visual overview is shown. After that, the process flow diagrams are given to enhance transparency about the modelling inside of Brightway / Activity Browser.
Both reactors are mainly based on (Brendelberger, 2024) and (Weber et al., 2023).
They both include a reduction and oxidation chamber, transport systems and the redox material. Furthermore, additional system-specific components have been modelled. It is assumed that the components are mostly constructed on site. Allocations are not included in both systems. The functional unit is 1 kg of produced hydrogen (at ambient pressure).

4.1 Monolithic System

Figure 5 shows the system boundary of the monolithic system. Special components in these boundaries are the RMA heat exchanger, the gates, the apertures, the vacuum pump as well as an heat exchanger for cooling the oxygen that has to be removed from the reduction chamber.

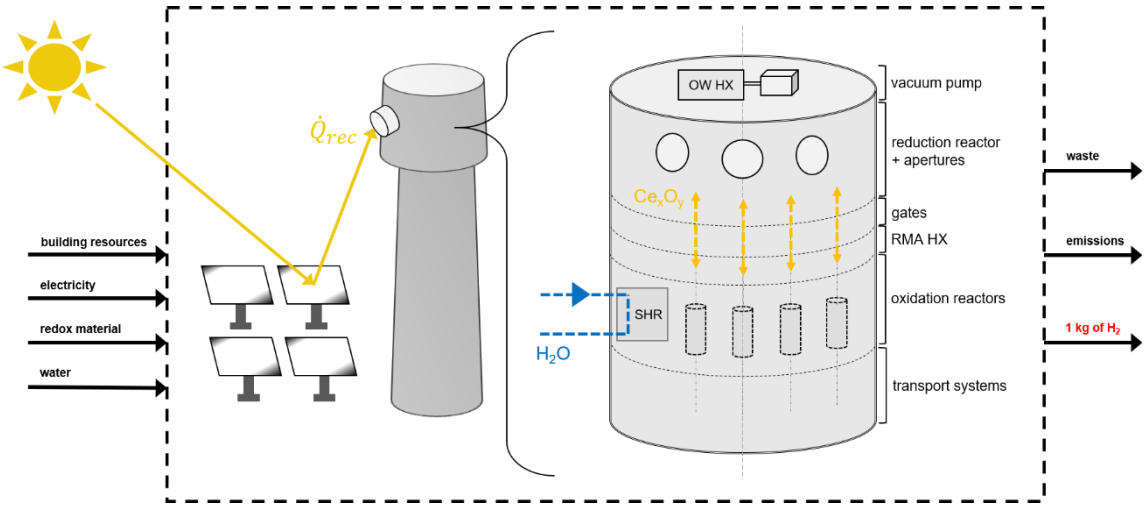

Figure 5: System boundary (monolithic system)

The process flow diagram of the monolithic system can be seen in Figure 6.
The construction materials of the reactor include the redox material, insulation, steel sheet, uncoated glass as well as pre-assembled parts for the transport systems and vacuum pump. Additionally, a steam heat recovery system and a heat exchanger for cooling the pumped oxygen are inside the system boundaries. These heat exchangers are modelled using ecoinvent data based on (Telsnig, 2015) as well. The heat exchanger from the original dataset are designed for molten salt and steam. Their mass and material flows are scaled linearly based on the heat flow that has to be transferred in both components.
These materials plus the ones used in the solar field and tower are transported to the site to be assembled. The use phase includes the electricity consumption of transport systems, vacuum pump and the heliostats as well as the water input and replacement of redox material. The EoL consists of the deconstruction and transport to the disposal, which is assumed to be either landfill or waste incineration.

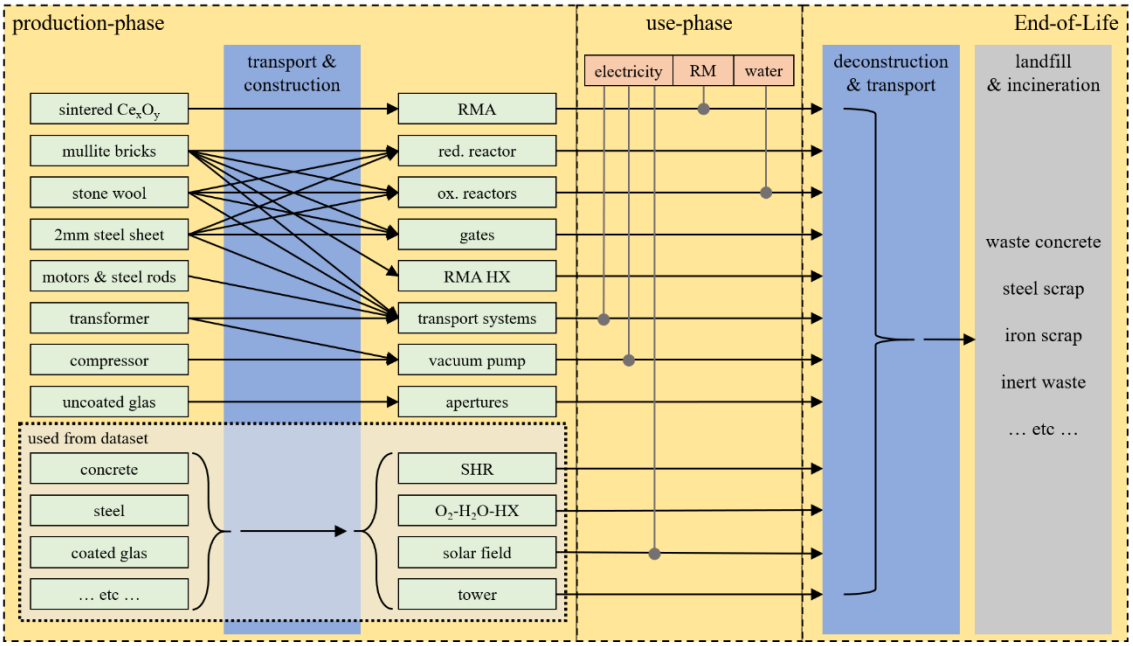

Figure 6: Process flow diagram (monolithic system)

4.2 Particle-Based System

In Figure 7, the system boundary of the particle-based system is shown.

Special components in these boundaries are the ITM, compressor and an aperture steam generation system used to recover heat from spillage around the receiver.

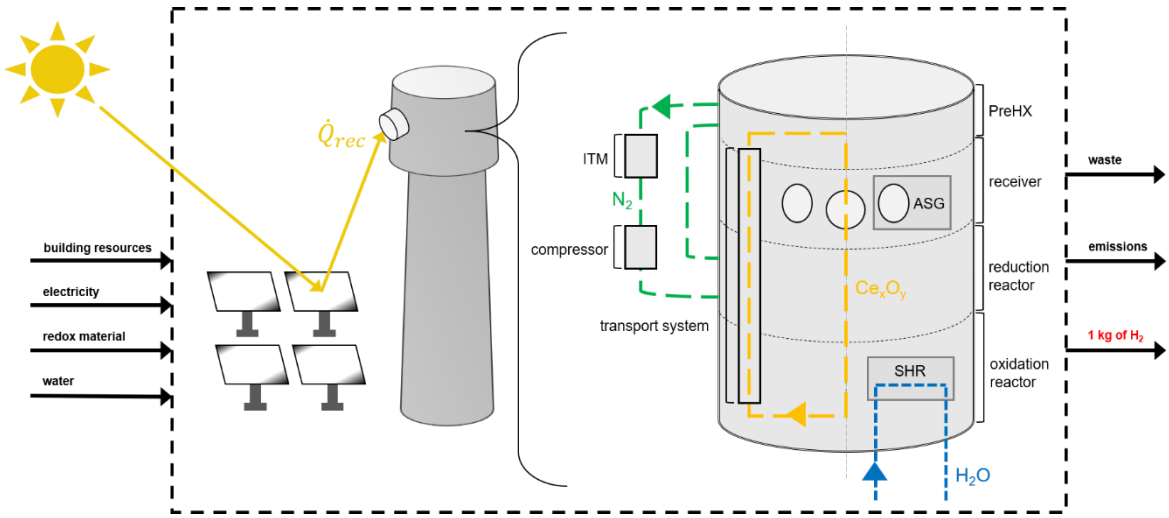

Figure 7: System boundary (particle-based system)

The process flow chart of this system, as illustrated in Figure 8, is structurally similar to the corresponding diagram of the monolithic system but differs in some respects.
Instead of using the heat from the vacuumed oxygen to heat up water, the aperture steam generation system is used. It is modelled based on (Telsnig, 2015) as well, just like the SHR system. The ion transport membrane consists of ceramic membranes, insulation, a steel casing and a transformer. In addition to the electrical consumption described for the monolithic system, the power required for running the ITM in the use-phase is also inside of the system boundaries. The End-of-Life is comparable to the monolithic system.

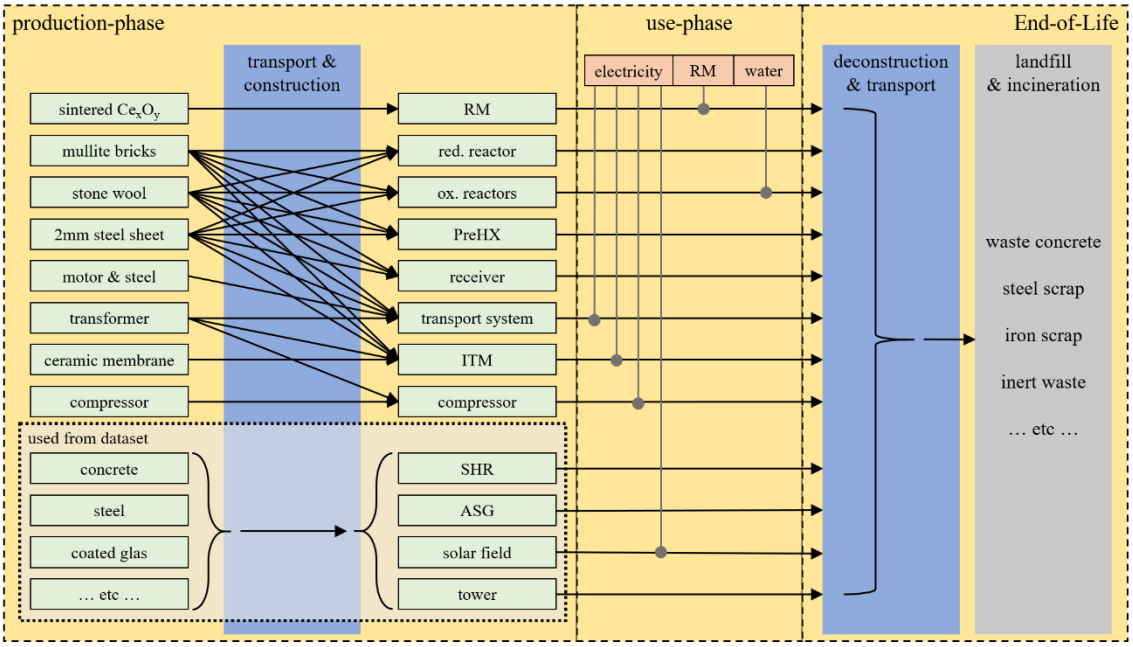

Figure 8: Process flow diagram (particle-based system)

5 Data and System Assumptions

In this chapter, information about data sources are shown as well as the assumptions made for both systems. First, requirements for the data are stated regarding coverage of time, geography and technology as well as consistency and reproducibility.

5.1 Data Quality Requirements

This study does not aim for quantitatively accurate results but rather a qualitative evaluation of the most important aspects for future research. However, the data sources should be as close to the present as possible to enhance the quality of the LCA.
The location at which a product is produced can greatly affect its environmental impact. Then again, as many processes are having large, global supply chains, geographical coverage is not assumed to be as important, especially because the location of choice in this study is purely exemplary. Technological coverage however is seen as relatively important as the concepts analyzed in this study are distinct in many aspects compared to other hydrogen production technologies. For both systems, it is tried to apply the presented methodology uniformly. Other than some exceptions (like the compressors or solar field and tower for example) geometrical simplification seems to be applicable to most components. As this work should be able to encourage further research, it should also be as reproducible as possible. This means that the parametrization and geometrical layout of the components are tried to be kept transparent.

5.2 Primary & Secondary Data

For conducting the study, mostly secondary data is used. This includes research papers from digital libraries as well as books. For information about the LCA software or the DNI for example, internet resources are referenced. As a data source for performing the LCA, the ecoinvent 3.9.1 database (ecoinvent, 2022) is used in combination with Brightway2 (Brightway Developers, 2025) and Activity-Browser (Steubing et al., 2025). Except for power consumption in the use-phase, most processes have RoW or GLO set as a location. Monolithic and particle-based system include a solar tower and heliostat field, which are modelled using an ecoinvent dataset based on (Telsnig, 2015). Primary data consists of talks or group meetings with colleagues from the institute.

5.3 Assumptions and System Modeling

In this section, the most important assumptions of both systems are explained. Additional values and the references taken for parametrization are given in the attachments.
The component dimensions and process-relevant parameters are taken from literature or internal discussions. Physical formulas are partly referenced from (Wetteborn, 2022) and (Brummund, 2022). The presumed geometry is shown in the attachments. The EoL phase is assumed to consist of landfilling or incineration.
To remain comparability, some physical properties of the two reactor concepts are set to the same value. The lifetime of both systems is fixed to 25 years, as this seemed reasonable to other LCA studies on H_2-production technologies or CSP (Ishaq and Dincer, 2024; Li et al., 2019; Mehmeti et al., 2018). The heat flow at the receiver / apertures is set to 150MW. At a default solar-to-fuel efficiency of 10% for the systems, this yields a H_2-production-rate of around 377.62 kg/h, which seems to be fitting to the consumption of further processing into synthetic fuels. The chosen solar-to-fuel efficiency is fairly uncertain, but seemed to be a good assumption on average considering (Wang et al., 2022; Weber et al., 2023) (higher efficiencies are theoretically possible however). As this results in fairly large components, further research could investigate splitting the systems into multiple smaller reactors. It is assumed the reactors would operate at the assumed heat input for 8 hours per day, which seems to be in the range presented by (Winter et al., 1991). As a location, Spain is chosen, as many CSP projects are situated there (Alami et al., 2023). This affects the DNI and electricity drawn in the use-phase. In reality, electrical power consumption would likely be covered by nearby renewable energy sources, so this should be implemented accordingly in future LCA-work. The transport is modelled using >32t EURO4 freight lorries, with an average transport distance of 200km. The construction and deconstruction are represented by operating diesel machines with a high load factor >74.57kW. Their operation time is approximated by dividing a building time of 2 years by the cumulated mass of the system. This yields a specific machine operation time of about 1.52 s/kg. It is assumed the components are welded along their perimeters. As the specific insulation material proposed by research on both technologies is not available in the ecoinvent database, a new process is modelled in the Activity-Browser to approach the thermal properties needed.

At a thickness of 20cm (Brendelberger, 2024), a mix of 65% mullite and 35% stone wool yields an insulation resistance of around 1.881 W/m^{2}K using physical properties taken from (Stephan et al., 2019). This is in range of the required value. Mullite is chosen as it seemed to be a fitting material considering (Brulin et al., 2022). It is modelled separately by modifying a clay production process. Instead of clay, a mixture of 74% aluminum oxide and 26% sand is assumed as the process input (Kumazawa and Suzuki, 2021). As the specific heat capacities of mullite and clay are similar (Et-tanteny et al., 2024; Hildmann and Schneider, 2004; Zhang et al., 2025), but the sintering temperatures are not (Kumazawa and Suzuki, 2021; Mahmoud et al., 2024), the consumption of natural gas was increased by factor of about 3.257 to account for the higher heating power. As no other steel sheet dataset was available in the database, the sheet thickness is assumed to be 2mm for all simplified components. The compressor and vacuum pump are modelled using multiple units of 300kW compressors from an ecoinvent dataset. Thereby, the amount is based on the power required for both components. For the components which consume electricity (e.g. compressor, vacuum pump, etc.), transformers are added. The specific weight of the transformers is assumed to be 500 kg per MW of power transformed. The water consumption of the systems is set to the same amount of hydrogen produced, i.e. all the water is split into H_2 and oxygen. The power required for pumping the water can be evaluated by equation (6):

$$P_{el,waterpump} = \frac{\eta_{stf} \times \dot{Q}_{rec} \times M_{H_2O} \times g \times h_{tower}}{\eta_{waterpump} \times HHV_{H_2}} \quad (6)$$

Even for very low pumping efficiencies and a tower height of 200m, this power is around 10kW for both systems, which makes the component neglectable compared to the other electrical power consumptions which are two magnitudes above it.
The heat required for turning the water into steam is described by equation (7):

$$\dot{Q}_{H_2O} = \frac{\eta_{stf} \times \dot{Q}_{rec}}{HHV_{H_2}} \times \left((373K - T_{amb}) \times c_{p,H_2O,l} + h_{H_2O,lg} + (T_{ox} - 373K) \times c_{p,H_2O,g}\right) \quad (7)$$

Using thermal properties taken from (Brendelberger, 2024) for water and assuming the parameter values given in the attachments, this results in a required heat flow of 5.19MW in the monolithic system and 5.04MW in the particle based reactor.

The transport systems are modelled using electrical vehicle motors with an efficiency of 80% (De Souza et al., 2024) and an average power density of 2000 W/kg (Gmyrek, 2024). The formula for determining the power consumption of the transport systems is given in equation (8):

$$P_{el,ts} = \frac{\dot{m}_{RM} \times g \times h}{\eta_{ts}} \quad (8)$$

The optical efficiency of the solar field and the spillage of heat on the receiver are based on (Weber et al., 2023). The area-specific electrical power consumption of the heliostats is determined using data from (Telsnig et al., 2017). The efficiency of the steam heat recovery is taken from (Brendelberger, 2024). The porosity of the redox material as well as the partial oxygen pressure in the reduction reactors are assumed to be the same for both systems. The lifetime of the cerium oxide is set to half a year and it is assumed that the RM is completely replaced with new material after this duration. However, (Rhodes et al., 2015) showed that the reduction extent of ceria only fell to 86.4% after 2000 cycles with the parametrization used in their study. This indicates a much longer material lifetime in reality as well as the option to recycle the used redox material. This should be investigated in further research for realistic assumptions about the RM. The processing of redox material is modelled using an iron sintering process and replacing the material input with cerium oxide. Oher flows were not adjusted for this process. The reduction extent is determined using a formula taken from (Bulfin et al., 2013).

It is shown in equation (9):

$$\delta = 0.35 \times \left(\left(\frac{\left(0.00001 \times \frac{p_{O_2,red}}{[Pa]}\right)^{0.217} \times e^{\left(\frac{195600 \frac{J}{mol}}{R \times T_{red}}\right)}}{8700} \right) + 1 \right)^{-1} \quad (9)$$

A relation between the required redox material flow and the reduction extent can be derived. It is given in equation (10):

$$\dot{m}_{CeO_2} = \frac{\eta_{stf} \times \dot{Q}_{rec} \times M_{CeO_2}}{HHV_{H_2} \times \delta} \quad (10)$$

Given that, the mass of cerium oxide and therefore the dimension of components in the systems change based on the required redox material for a certain velocity.
Next, further assumptions specifically made for the monolithic system are described.
It is assumed that the oxygen produced in the reduction reactor is cooled down to a temperature of 60°C before entering the vacuum pump. The VP is assumed to have an efficiency of 50%, which seems reasonable considering (Liao et al., 2025), but there is a high degree of uncertainty. The power consumption is calculated using equation (10):

$$P_{el,VP} = \frac{\eta_{stf} \times \dot{Q}_{rec} \times R \times T_{VP} \times \ln\left(\frac{p_{O_2,out}}{p_{O_2,in}}\right)}{\eta_{VP} \times HHV_{H_2}} \quad (10)$$

As the heat taken from the vacuumed oxygen must be at least equal to the remaining power required for heating up the water, it is checked by using equation (11), in which the heat capacity of oxygen is taken from (Stephan et al., 2019).

$$\dot{Q}_{O_2} = \frac{\eta_{stf} \times \dot{Q}_{rec}}{2 \times HHV_{H_2}} \times (T_{red} - T_{VP}) \times c_{p,O_2} \approx 1.43MW > (1 - \eta_{shr}) \times \dot{Q}_{H_2O} \approx 519kW \quad (11)$$

The gates are set to a fixed height which is not dependent on the amount of redox material. The number & dimension of the apertures are fixed as well. The RMA heat exchanger is assumed to consist completely out of mullite. The RMA is presumed to be cylindrical as shown in (Brendelberger, 2024) and its height varies depending on the mass required in the system. This height then affects the dimension of other components like the reduction and oxidation reactor as well as the transportation systems.
Now, assumptions specific to the particle-based system are shown. The components are assumed to only be filled by 20%, although this fraction is possibly higher in reality. The bed porosity was set to a uniform value.

It is assumed that there is just one reduction reactor instead of multiple chambers. The used CSP-dataset is taken partly for modelling the ASG. It includes a cement bonded particle board, which is split in cement and wood for the EoL phase at a relation referenced from (Wang et al., 2016). The height of reduction and oxidation reactor as well as the preheating heat exchanger and transport system is scaled proportionally to a fixed residence time and particle velocity. This goes back to (Weber et al., 2023) and can be seen in equation (12):

$$h \sim \frac{t_{res} \times \dot{m}_{CeO_2}}{\rho_{CeO_2} \times r_{bed}^2 \times \pi \times (1 - \varphi_{bed})} \quad (12)$$

Thereby, the bed radius is fixed for the components. To account for 150MW of heat flow, it was assumed that there are 4 receivers of which the dimensions are known. The bed height in the receivers is assumed to be 4.2 times the diameter of the particles. The rotation systems of the receivers are not included in the system boundaries, as the energy required for making them turn is considered negligible. This energy consumption (disregarding friction) can be calculated for the whole lifetime, as shown in equation (13). The receivers are assumed to be accelerated to the desired speed each day.

$$W_{el,rec,rot,lt} = n_{rec} \times \frac{\left(m_{sc,rec} + m_{ins,rec}\right) \times r_{rec,i}^2 \times \left(\frac{2\pi}{T_{rec,rot}}\right)^2}{2 \times \eta_{rot}} \times 365 \frac{d}{yr} \times t_{lt} \quad (13)$$

Even assuming a short duration of 5s per rotation and the parametrization shown in the attachments, this gives an electrical energy consumption of less than 3.5 MWh, making it neglectable compared to the other power consumptions. The transport system is scaled by a certain factor (0.5 in this study) relative to the bed radius, which affects every sub-component inside of it. The power consumptions of compressor and ion transport membrane are scaled linearly based on values given for a smaller concept, as it is assumed that these power requirements are proportional to the production rate of hydrogen.
For the production of membrane material inside of the ITM, a clay ceramic production dataset from the ecoinvent database is used.

Instead of clay, lanthanum oxide is taken as an input. Combustion energy is not adjusted. Although simplified, lanthanum oxide seems to be a reasonable material considering (Nemitallah et al., 2013; Noviyanti et al., 2021; Sunarso et al., 2017). The oxygen permeability of the membrane is determined using a formula taken from (Sunarso et al., 2017). It is shown in equation (14):

$$J_{O_2} = \frac{R \times T_{ox}}{16 \times F^2 \times d_{cm}} \times \sigma_{ionic} \times \ln\left(\frac{p_{O_2,rich}}{p_{O_2,lean}}\right) \quad (14)$$

Assuming a membrane thickness of around 1mm (Nemitallah et al., 2013), an ionic conductivity of 1.6 S/m (Noviyanti et al., 2021), a partial oxygen pressure of 21% of atmospheric pressure at the rich side an 100 Pa at the lean side, this yields an oxygen permeability of approximately 540 µmol*m^{-2}*s^{-1}. However, the ionic conductivity has an especially high degree of uncertainty, as it varies depending on the specific chemical composition of the membrane material (Noviyanti et al., 2021). The value used is more valid for compositions including tin or bismuth. For more accurate results this should be regarded when modelling the production process in the future. Using the oxygen permeability, the volume of the ceramic membrane can be evaluated using equation (15):

$$V_{ITM,cm} = \frac{d_{cm} \times \eta_{stf} \times \dot{Q}_{rec}}{2 \times J_{O_2} \times HHV_{H_2}} \quad (15)$$

To account for the spacing between the membrane layers, it is assumed that the total inner volume of the ITM component is four times $V_{ITM,cm}$. As there is no vacuum pumping involved in the particle-based system, the remaining heat required for heating the water is assumed to come from spillage around the receivers. Using equation (16), which goes partly back to (Weber et al., 2023), it can be checked whether the spillage is high enough:

$$\dot{Q}_{spillage} = \frac{1-\eta_{rec}}{\eta_{rec}} \times \dot{Q}_{rec} \approxeq 64.29MW \gg (1-\eta_{shr}) \times \dot{Q}_{H_2O} \approxeq 504kW \quad (16)$$

Sweep gas leakage is not considered. Because of that, an air separation unit is not included in the system boundaries. Detailed information about the dimensioning of solar tower and field are given in the attachments.

6 Conclusion

In this study, an LCA-based methodology according to ISO norms has been developed, serving for the evaluation of most important research deficits as well as a template for further environmental assessment. The implementation of flexible LCA-models inside of Brightway2 / Activity Browser was successful and has proven to be helpful. Thereby, the geometry of most components was simplified, allowing the usage of formulas to calculate mass flows. A monolithic and particle-based reactor concept were evaluated on their environmental life cycle impact from a cradle-to-grave perspective, whereas no recycling was considered. The data quality is presumed to be mostly sufficient in terms of temporal coverage. As many assumptions are very likely to diverge from real-world scenarios (e.g. material properties or electricity source), the obtained results do however not allow comparability to other H_2-production technologies yet. Instead, recommendations for the focus of further research can be given. The life cycle impact assessment has revealed the components which contribute the most to the environmental impact. In the case of the monolithic system, this turned out to be the redox material assembly as well as the transport systems for example. For the particle-based system, the redox material and the production of the ion transport membrane are found to be the most important. It must be said that the components which consume electrical power will probably have a lower environmental impact in reality and are not named here, as the energy will not be drawn from the electricity grid, but rather renewable sources or waste heat. The sensitivity analysis has shown that the average transport distance only has a low influence on the LCIA, while solar-to-fuel efficiency and redox material lifetime can have a high effect on the results. The sensitivity on location may not be as important, as the systems would likely be energy-autonomous. To conclude, a flexible methodology for the iterative environmental assessment of the analyzed technologies was worked out. However, the improvement of redox material durability, the usage of renewable electricity, the increasing of solar-to-fuel efficiency as well as recycling of components should be addressed in further research to attain accurate LCIA results. If these aspects are improved and investigated further from an LCA-perspective, thermochemical redox-cycling is a promising production concept for renewable and clean hydrogen production.

7 References

Alami, A.H., Olabi, A.G., Mdallal, A., Rezk, A., Radwan, A., Rahman, S.M.A., Shah, S.K., Abdelkareem, M.A., 2023. Concentrating solar power (CSP) technologies: Status and analysis. Int. J. Thermofluids 18, 100340. https://doi.org/10.1016/j.ijft.2023.100340

Brendelberger, S., 2024. R2Mx plant model for solar thermochemical hydrogen production at MW scale. Int. J. Hydrog. Energy 91, 1407–1421. https://doi.org/10.1016/j.ijhydene.2024.10.050

Brendelberger, S., Holzemer-Zerhusen, P., Vega Puga, E., Roeb, M., Sattler, C., 2022. Study of a new receiver-reactor cavity system with multiple mobile redox units for solar thermochemical water splitting. Sol. Energy 235, 118–128. https://doi.org/10.1016/j.solener.2022.02.013

Brendelberger, S., Von Storch, H., Bulfin, B., Sattler, C., 2017. Vacuum pumping options for application in solar thermochemical redox cycles – Assessment of mechanical-, jet- and thermochemical pumping systems. Sol. Energy 141, 91–102. https://doi.org/10.1016/j.solener.2016.11.023

Brightway Developers, 2025. Brightway Documentation [WWW Document]. URL https://docs.brightway.dev/en/latest/ (accessed 16.2.25)

Brulin, J., Gasser, A., Rekik, A., Blond, E., Roulet, F., 2022. Thermomechanical modelling of a blast furnace hearth. Constr. Build. Mater. 326, 126833. https://doi.org/10.1016/j.conbuildmat.2022.126833

Brummund, U., 2022. E2: Physik (Lecture at Hochschule Bonn-Rhein-Sieg University of Applied Sciences).

Brundtland et al., 1987. Report of the World Commission on Environment and Development “Our Common Future.” https://digitallibrary.un.org/record/139811?v=pdf

Bulfin, B., Lowe, A.J., Keogh, K.A., Murphy, B.E., Lübben, O., Krasnikov, S.A., Shvets, I.V., 2013. Analytical Model of CeO_2 Oxidation and Reduction. J. Phys. Chem. C 117, 24129–24137. https://doi.org/10.1021/jp406578z

Chang, D., Lee, C.K.M., Chen, C.-H., 2014. Review of life cycle assessment towards sustainable product development. J. Clean. Prod. 83, 48–60. https://doi.org/10.1016/j.jclepro.2014.07.050

Chelvam, K., Hanafiah, M.M., Woon, K.S., Ali, K.A., 2024. A review on the environmental performance of various hydrogen production technologies: An approach towards hydrogen economy. Energy Rep. 11, 369–383. https://doi.org/10.1016/j.egyr.2023.11.060

Chen, C., Jiao, F., Lu, B., Liu, T., Liu, Q., Jin, H., 2023. Challenges and perspectives for solar fuel production from water/carbon dioxide with thermochemical cycles. Carbon Neutrality 2, 9. https://doi.org/10.1007/s43979-023-00048-6

Cho, H.H., Strezov, V., Evans, T.J., 2023. A review on global warming potential, challenges and opportunities of renewable hydrogen production technologies. Sustain. Mater. Technol. 35, e00567. https://doi.org/10.1016/j.susmat.2023.e00567

De Souza, D.F., Da Silva, P.P.F., Sauer, I.L., De Almeida, A.T., Tatizawa, H., 2024. Life cycle assessment of electric motors - A systematic literature review. J. Clean. Prod. 456, 142366. https://doi.org/10.1016/j.jclepro.2024.142366

DIN EN ISO 14040:2021-02, Umweltmanagement_- Ökobilanz_- Grundsätze und Rahmenbedingungen (ISO_14040:2006_+ Amd_1:2020); Deutsche Fassung EN_ISO_14040:2006_+ A1:2020, 2021. https://doi.org/10.31030/3179655

DIN EN ISO 14044:2021-02, Umweltmanagement_- Ökobilanz_- Anforderungen und Anleitungen (ISO_14044:2006_+ Amd_1:2017_+ Amd_2:2020); Deutsche Fassung EN_ISO_14044:2006_+ A1:2018_+ A2:2020, 2021. https://doi.org/10.31030/3179656

ecoinvent, 2025. ecoinvent Knowledge Base [WWW Document]. URL https://support.ecoinvent.org/ecoinvent-version-3.9.1 (accessed 16.2.25).

ecoinvent, 2022. ecoinvent database 3.9.1. https://support.ecoinvent.org/ecoinvent-version-3.9.1

Elsayed Elfeky, K., Hosny, M., Abu Khatwa, S., Gambo Mohammed, A., Wang, Q., 2024. CSP plants cooling technology: Techno-economic analysis, parametric study, and stacking ensemble learning forecasting. Therm. Sci. Eng. Prog. 54, 102777. https://doi.org/10.1016/j.tsep.2024.102777

Emetere, M.E., Oniha, M.I., Akinyosoye, D.A., Elughi, G.N., Afolalu, S.A., 2024. Progress and challenges of green hydrogen gas production: Leveraging on the successes of biogas. Int. J. Hydrog. Energy 79, 1071–1085. https://doi.org/10.1016/j.ijhydene.2024.07.115

Et-tanteny, R., El Amrani, B., Manssouri, I., Limami, H., 2024. Physicochemical, mechanical and thermal analysis of unfired clay bricks: Kaolinite-PEG 6000 composite. Clean. Eng. Technol. 22, 100793. https://doi.org/10.1016/j.clet.2024.100793

Feng, H., Zhao, J., Hollberg, A., Habert, G., 2023. Where to focus? Developing a LCA impact category selection tool for manufacturers of building materials. J. Clean. Prod. 405, 136936. https://doi.org/10.1016/j.jclepro.2023.136936

François, A., Roche, R., Grondin, D., Winckel, N., Benne, M., 2024. Investigating the use of hydrogen and battery electric vehicles for public transport: A technical, economical and environmental assessment. Appl. Energy 375, 124143. https://doi.org/10.1016/j.apenergy.2024.124143

Frischknecht, R., Rebitzer, G., 2005. The ecoinvent database system: a comprehensive web-based LCA database. J. Clean. Prod. 13, 1337–1343. https://doi.org/10.1016/j.jclepro.2005.05.002

Gerhardt-Mörsdorf, J., Peterssen, F., Burfeind, P., Benecke, M., Bensmann, B., Hanke-Rauschenbach, R., Minke, C., 2024. Life Cycle Assessment of a 5 MW Polymer Exchange Membrane Water Electrolysis Plant. Adv. Energy Sustain. Res. 5, 2300135. https://doi.org/10.1002/aesr.202300135

Global Solar Atlas [WWW Document], 2025. URL https://globalsolaratlas.info/map (accessed 16.2.25).

Gmyrek, Z., 2024. Optimal Electric Motor Designs of Light Electric Vehicles: A Review. Energies 17, 3462. https://doi.org/10.3390/en17143462

Hildmann, B., Schneider, H., 2004. Heat Capacity of Mullite - New Data and Evidence for a High-Temperature Phase Transformation. J. Am. Ceram. Soc. 87, 227–234. https://doi.org/10.1111/j.1551-2916.2004.00227.x

Huijbregts, M.A.J., Steinmann, Z.J.N., Elshout, P.M.F., Stam, G., Verones, F., Vieira, M., Zijp, M., Hollander, A., Van Zelm, R., 2017. ReCiPe2016: a harmonised life cycle impact assessment method at midpoint and endpoint level. Int. J. Life Cycle Assess. 22, 138–147. https://doi.org/10.1007/s11367-016-1246-y

Institute of Future Fuels, 2025a. The Institute of Future Fuels [WWW Document]. DLR Website. URL https://www.dlr.de/en/ff/about-us/the-institute-of-future-fuels (accessed 16.2.25).

Institute of Future Fuels, 2025b. SOLHYKO [WWW Document]. DLR Website. URL https://www.dlr.de/en/ff/research-and-transfer/projects/2023/solhyko (accessed 16.2.25).

Ishaq, M., Dincer, I., 2024. A cradle-to-gate life cycle assessment for clean hydrogen gas production pathway using the CeO2/Ce2O3-based redox thermochemical cycle. Gas Sci. Eng. 131, 205464. https://doi.org/10.1016/j.jgsce.2024.205464

Kafle, S., Sapkota, S., Higgins, B.T., Adhikari, S., 2025. Research trends in life cycle assessment of hydrogen production: Methodological review on thermochemical conversion processes. Int. J. Hydrog. Energy 106, 432–443. https://doi.org/10.1016/j.ijhydene.2025.01.472

Kodgire, P., 2025. Hydrogen - imminent clean and green energy: Hydrogen production technologies life cycle assessment review. Process Saf. Environ. Prot. 193, 483–500. https://doi.org/10.1016/j.psep.2024.11.019

Kumazawa, T., Suzuki, H., 2021. Transient liquid phase sintering of high-purity mullite for high-temperature structural ceramics. Ceram. Int. 47, 12381–12388. https://doi.org/10.1016/j.ceramint.2021.01.092

Le Gal, A., Vallès, M., Julbe, A., Abanades, S., 2022. Thermochemical Properties of High Entropy Oxides Used as Redox-Active Materials in Two-Step Solar Fuel Production Cycles. Catalysts 12, 1116. https://doi.org/10.3390/catal12101116

Li, R., Zhang, H., Wang, H., Tu, Q., Wang, X., 2019. Integrated hybrid life cycle assessment and contribution analysis for CO2 emission and energy consumption of a concentrated solar power plant in China. Energy 174, 310–322. https://doi.org/10.1016/j.energy.2019.02.066

Liao, Y., Wright, A., Li, J., 2025. Simulation and optimisation of vacuum (pressure) swing adsorption with simultaneous consideration of real vacuum pump data and bed fluidisation. Sep. Purif. Technol. 358, 130354. https://doi.org/10.1016/j.seppur.2024.130354

Mahmoud, K.A., Kapustin, F.L., Shironina, A.M., Cholakh, S.O., Voronin, I.P., Abdel-Azeem, M.M., Ismail, A.M., Mira, H.I., Tashlykov, O.L., 2024. Experimental investigation of the annealing temperature impacts on the physical, morphological, and gamma-ray attenuation properties of clay-based bricks. Radiat. Phys. Chem. 223, 111932. https://doi.org/10.1016/j.radphyschem.2024.111932

Mehmeti, A., Angelis-Dimakis, A., Arampatzis, G., McPhail, S., Ulgiati, S., 2018. Life Cycle Assessment and Water Footprint of Hydrogen Production Methods: From Conventional to Emerging Technologies. Environments 5, 24. https://doi.org/10.3390/environments5020024

Mutel, C., 2017. Brightway GitHub [WWW Document]. URL https://github.com/brightway-lca/brightway2/blob/master/notebooks/Getting%20Started%20with%20Brightway2.ipynb (accessed 16.2.25).

National Oceanic and Atmospheric Administration, 2025. Annual anomalies in global land and ocean surface temperature from 1880 to 2024, based on temperature departure (in degrees Celsius) [WWW Document]. Stat. Inc. URL https://www.statista.com/statistics/224893/land-and-ocean-temperature-anomalies-based-on-temperature-departure/ (accessed 16.2.25).

Nemitallah, M.A., Habib, M.A., Mansour, R.B., 2013. Investigations of oxy-fuel combustion and oxygen permeation in an ITM reactor using a two-step oxy-combustion reaction kinetics model. J. Membr. Sci. 432, 1–12. https://doi.org/10.1016/j.memsci.2012.12.028

Noviyanti, A.R., Juliandri, Winarsih, S., Syarif, D.G., Malik, Y.T., Septawendar, R., Risdiana, 2021. Highly enhanced electrical properties of lanthanum-silicate-oxide-based SOFC electrolytes with co-doped tin and bismuth in $La_{9.33-x}\ Bi_x\ Si_{6-y}\ Sn_y\ O_{26}$. RSC Adv. 11, 38589–38595. https://doi.org/10.1039/D1RA07223D

Rhodes, N.R., Bobek, M.M., Allen, K.M., Hahn, D.W., 2015. Investigation of long term reactive stability of ceria for use in solar thermochemical cycles. Energy 89, 924–931. https://doi.org/10.1016/j.energy.2015.06.041

Rihner, M.C.S., Whittle, J.W., Gadelhaq, M.H.A., Mohamad, S.N., Yuan, R., Rothman, R., Fletcher, D.I., Walkley, B., Koh, L.S.C., 2025. Life cycle assessment in energy-intensive industries: Cement, steel, glass, plastic. Renew. Sustain. Energy Rev. 211, 115245. https://doi.org/10.1016/j.rser.2024.115245

Rizvi, A.A., Danish, S.N., El-Leathy, A., Al-Ansary, H., Yang, D., 2021. A review and classification of layouts and optimization techniques used in design of heliostat fields in solar central receiver systems. Sol. Energy 218, 296–311. https://doi.org/10.1016/j.solener.2021.02.011

Song, Z., Liu, C., 2022. Energy efficient design and implementation of electric machines in air transport propulsion system. Appl. Energy 322, 119472. https://doi.org/10.1016/j.apenergy.2022.119472

Stephan, P., Kabelac, S., Kind, M., Mewes, D., Schaber, K., Wetzel, T. (Eds.), 2019. VDI-Wärmeatlas: Fachlicher Träger VDI-Gesellschaft Verfahrenstechnik und Chemieingenieurwesen, Springer Reference Technik. Springer Berlin Heidelberg, Berlin, Heidelberg. https://doi.org/10.1007/978-3-662-52989-8

Steubing, B., de Koning, D., Haas, A., Mutel, C.L., 2020. The Activity Browser — An open source LCA software building on top of the brightway framework. Softw. Impacts 3, 100012. https://doi.org/10.1016/j.simpa.2019.100012

Steubing, B., Visscher, M., 2025. Activity-Brower GitHub [WWW Document]. URL https://github.com/LCA-ActivityBrowser/activity-browser (accessed 16.2.25).

Steubing, B., Visscher, M., van der Meide, M., for contributors: see https://github.com/LCA-ActivityBrowser/activity-browser, 2025. Activity Browser.

Strelkovskii, N., Komendantova, N., 2025. Integration of UN sustainable development goals in national hydrogen strategies: A text analysis approach. Int. J. Hydrog. Energy 102, 1282–1294. https://doi.org/10.1016/j.ijhydene.2025.01.134

Sunarso, J., Hashim, S.S., Zhu, N., Zhou, W., 2017. Perovskite oxides applications in high temperature oxygen separation, solid oxide fuel cell and membrane reactor: A review. Prog. Energy Combust. Sci. 61, 57–77. https://doi.org/10.1016/j.pecs.2017.03.003

Telsnig, T., 2015. Standortabhängige Analyse und Bewertung solarthermischer Kraftwerke am Beispiel Südafrikas. Universität Stuttgart.

Telsnig, T., Weinrebe, G., Finkbeiner, J., Eltrop, L., 2017. Life cycle assessment of a future central receiver solar power plant and autonomous operated heliostat concepts. Sol. Energy 157, 187–200. https://doi.org/10.1016/j.solener.2017.08.018

United Nations, 2025. Department of Economic and Social Affairs - Sustainable Development [WWW Document]. URL https://sdgs.un.org/goals (accessed 16.2.25).

United Nations General Assembly, 2024. Progress towards the Sustainable Development Goals. https://unstats.un.org/sdgs/files/report/2024/SG-SDG-Progress-Report-2024-advanced-unedited-version.pdf

Wang, B., Li, X., Dai, Y., Wang, C.-H., 2022. Thermodynamic analysis of an epitrochoidal rotary reactor for solar hydrogen production via a water-splitting thermochemical cycle using nonstoichiometric ceria. Energy Convers. Manag. 268, 115968. https://doi.org/10.1016/j.enconman.2022.115968

Wang, L., Chen, S.S., Tsang, D.C.W., Poon, C.S., Shih, K., 2016. Value-added recycling of construction waste wood into noise and thermal insulating cement-bonded particleboards. Constr. Build. Mater. 125, 316–325. https://doi.org/10.1016/j.conbuildmat.2016.08.053

Weber, A., Grobbel, J., Neises-von Puttkamer, M., Sattler, C., 2023. Swept open moving particle reactor including heat recovery for solar thermochemical fuel production. Sol. Energy 266, 112178. https://doi.org/10.1016/j.solener.2023.112178

Wetteborn, K., 2022. A3: Thermodynamik und Wärmeübertragung (Lecture at Hochschule Bonn-Rhein-Sieg University of Applied Sciences).

Winter, C.-J., Sizmann, R.L., Vant-Hull, L.L. (Eds.), 1991. Solar Power Plants: Fundamentals, Technology, Systems, Economics. Springer Berlin Heidelberg, Berlin, Heidelberg. https://doi.org/10.1007/978-3-642-61245-9

Zhang, H., Zhang, Y., Han, S., Wu, K., Shen, X., 2025. Analysis on thermomechanical characteristics of refractory brick structure with different material properties and structure parameters in incinerators. Mater. Today Commun. 42, 111166. https://doi.org/10.1016/j.mtcomm.2024.111166

The following AI-tools were used for linguistic improvement to write this paper:

https://www.deepl.com/de/translator

https://www.deepl.com/de/write

https://chatgpt.com/